1	Effects of sea spray on the simulated tropical cyclone development:
2	Dependence on surface drag coefficient parameterization
3	Ziqiang Duan ^{1,2} , Yuqing Wang ^{3*} , and Yuanlong Li ⁴
4 5	¹ Shanghai Typhoon Institute and Key Laboratory of Numerical Modeling for Tropical Cyclone, China Meteorological Administration, Shanghai 200030, China
6	² Asia-Pacific Typhoon Collaborative Research Center, Shanghai 200030, China
7 8	³ Department of Atmospheric Sciences and International Pacific Research Center, School of Ocean and Earth Science and Technology, University of Hawaii at Manoa, Honolulu, HI 96822
9	⁴ School of Atmospheric Sciences, Nanjing University, Nanjing, China.
10 11 12 13 14	June 13, 2022 (submitted) August 18, 2022 (first revision) October 11, 2022 (second revision) November 30, 2022 (Third revision) Dateline
15	Key points:
16 17	1. The sea spray effect on TC intensity evolution depends on the surface drag (C _D) scheme used and the stages of the TC lifetime.
18 19	2. Different wind speed dependence of C _D can affect the radial distribution of the spray mass flux and thus spray-mediated enthalpy flux.
20 21	3. Although spray can speed up or slow down the intensification rate, it contributes positively to the mature-stage TC intensity.
22	Submitted to <i>Journal of Geophysical Research – Atmospheres</i>
23 24 25	* Corresponding author address: Prof. Yuqing Wang International Pacific Research Center
26	University of Hawaii at Manoa
272829	404A/POST, 1680 East West Road Honolulu, HI 96822, USA Email: yuqing@hawaii.edu

30 Abstract

31

32

33

34

35

36

37

38

39

40

41

42

43

44

45

46

47

48

Wave breaking under strong wind conditions in tropical cyclones (TCs) can generate sea spray droplets, which, during their suspension in air, release sensible heat due to the air-sea temperature difference while absorb sensible heat from the environment when they evaporate and release latent heat to the environment. Since the spray mass flux is a function of surface drag coefficient (C_D), the effect of spray on TC evolution should depends on C_D parameterization, while this has not been addressed so far. This study examines the effects of sea spray on the simulated TC evolution with two different C_D parameterizations (the WRF default scheme and the Donelan scheme). Results show that during the primary intensification stage, the TC with spray effect becomes stronger than that without spray when the WRF CD scheme is used, but becomes weaker when the Donelan CD scheme is used. This occurs because C_D is maximum outside the RMW with the Donelan scheme, which produces relatively large spray-mediated latent heat flux outside the RMW, which is unfavorable for TC intensification. The difference is enlarged by a feedback between spray and TC intensification involving the inertial stability and surface friction-induced radial inflow. However, in the mature stage, the simulated TCs with spray become stronger no matter which C_D scheme is used. In addition, the spray effect on the TC inner-core size evolution also weakly depends on the drag parameterization. When C_D is relatively greater outside the RMW, the inclusion of the spray effect would lead to the inner-core size increase.

Key words: Tropical cyclone, Sea spray, Drag coefficient, Sensible and latent heat fluxes

Plain Language Summary: Wave breaking under strong wind conditions, such as in tropical cyclones (TCs), can generate abundant sea spray droplets, which, during their suspension in air, release sensible heat due to the air-sea temperature difference while absorb sensible heat from the environment when they evaporate and release latent heat to the environment. This will mediate the air-sea enthalpy transfer and affect the TC intensification. As the spray mass flux is closely related with sea surface drag coefficient (C_D), we investigated how the spray effects on TC intensity evolution depend on the C_D scheme used in idealized numerical simulations. Two C_D schemes were used to perform four numerical experiments. Results show that the sea spray effect on TC intensity evolution depends on the C_D scheme used and the stages of the TC lifetime, largely due to the different wind speed dependence of C_D and its effect on the radial distribution of the spray-mediated latent flux. However, the finding demonstrates that caution should be given to surface drag parameterization when the sea spray effects on TC evolution are studied using numerical models. It is also suggested that efforts to measure spray properties under TC conditions should be conducted to validate/improve spray parameterization in the future.

1. Introduction

64

65

66

67

68

69

70

71

72

73

74

75

76

77

78

79

80

81

82

83

84

85

Sea spray droplets are abundantly generated by wave breaking under high near-surface wind conditions, such as in the boundary layer of tropical cyclones (TCs) (Mestayer & Lefauconnier, 1988; Rouault et al., 1991; Edson et al., 1996). During their suspension in air, sea spray droplets exchange heat and moisture with the surrounding air and mediate the air-sea enthalpy transfer, which may affect TC intensification and boundary layer structure (Andreas, 1992; Fairall et al., 1994; Andreas & Emanuel, 2001; Wang et al., 2001; Mueller & Veron, 2014a, 2014b). Sea spray releases sensible heat due to the air-sea temperature difference while absorbs sensible heat from the surrounding air when they evaporate and release latent heat to the air. The feedback of spray can change air moisture and temperature in the lower boundary layer, and indirectly affect the direct interfacial air-sea enthalpy flux (Fairall et al., 1994; Mueller & Veron, 2014b). Sea spray has been considered as an important factor affecting TC structure and intensity (Kepert et al., 1999; Andreas & Emanuel, 2001; Wang et al., 2001; Perrie et al., 2005; Gall et al., 2008; Bao et al., 2011; Ma et al., 2015). Surface drag coefficient (C_D) is an important parameter affecting TC development, structure, and the maximum intensity (Rosenthal, 1971; Montgomery et al., 2010; Thomsen et al., 2012; Peng et al., 2018; Li & Wang, 2021a). Most previous numerical studies (Craig and Gray, 1996; Montgomery et al., 2010; Thomsen et al., 2012; Peng et al., 2018; Li and Wang, 2021a) showed that the intensification rate of a TC simulated in state-of-the-art high-resolution numerical models is often insensitive to C_D but the maximum intensity is limited by C_D, as predicted by the theoretical maximum potential intensity (MPI) (Emanuel, 1986, 1995; Wang et al., 2021a, b). Montgomery et al. (2010) examined the sensitivity of the intensification of a simulated TC to C_D in a nonhydrostatic, three-dimensional, cloud-resolving model and showed that when C_D was less than 2.0×10^{-3} both the intensification rate and mature intensity of the simulated TC increased slightly with increasing C_D , but the mature intensity decreased for a larger C_D . Thomsen et al. (2012) found that both the intensification rate and mature intensity of the simulated TC were insensitive to C_D randomly perturbed by as large as 60%. Kilroy et al. (2017) showed that a relatively large C_D could accelerate the initial organization of deep convection in the inner core and thus shorten the initial spin-up stage of a simulated TC. In a more recent study, Li & Wang (2021a) found that although the initial spin-up of the simulated TC development was considerably shortened with a larger C_D , the subsequent intensification rate showed little difference while a larger C_D also shortened the intensification period, thus resulting a weaker steady-state intensity (see also the recent theoretical study by Wang et al. 2022).

In addition to its effect on the calculation of air-sea interfacial momentum flux directly, C_D also affects the air-sea enthalpy flux by modifying the spray mass flux. On the other hand, C_D can be also affected by wave-breaking. That means that wave and surface drag should be coupled (e.g., Chen et al., 2013). However, in practical applications, C_D is often parameterized as a function of near-surface wind speed with the dependence on wave breaking implicitly included. In the current version of the advanced Weather Research and Forecasting (WRF) model, C_D is a constant in the high-wind regime (greater than 30 m s⁻¹) for TC simulations. While some other studies indicated that C_D decreases with wind speed when wind speed exceeds about 30 m s⁻¹ (Powell et al., 2003; Makin, 2005; Black et al., 2007; Donelan, 2018), some recent studies have shown that C_D in the hurricane-force wind regime might be underestimated and the reduction in C_D may not be realistic (Richter et al., 2021). It is likely that some uncertainty remains in current C_D parameterization

schemes.

With different C_D schemes, the sea surface roughness and hence the spray mass flux are different (see section 2 for details). This means that the effects of spray on TC evolution may depend on the C_D scheme used in numerical simulations. Recently, Li & Wang (2021a) demonstrated that C_D can affect the radial location and strength of the maximum boundary layer inflow and eyewall updraft and thus eyewall convection. They showed that although the effect of C_D on the intensification rate during the primary intensification stage is not significant, C_D may considerably affect the onset time of the primary intensification and the final maximum intensity of the simulated TCs. Since C_D can affect the spray mass flux and the radial inflow, the different dependences of C_D on surface wind speed may affect the radial distribution of spray mass flux and thus the spray-mediated sensible and latent heat fluxes (namely enthalpy flux). Xu & Wang (2010) demonstrated that TC structure and intensity can be sensitive to the radial distribution of surface enthalpy flux. Therefore, the effect of spray on TC evolution may be different when different C_D parameterization schemes are employed in numerical simulations. However, this possibility has not been investigated in the literature.

This study attempts to examine the possible dependence of the quantity and distribution of sea spray-mediated fluxes on the C_D scheme used and the effect on the simulated TC structure and intensity evolution in idealized simulations. We will show that the different dependence of C_D on surface wind speed can result in different radial distributions and magnitudes of latent heat fluxes. Such effect is different in the intensification stage and the mature stage of the simulated TC, leading to either positive or negative effect on TC intensity in different stages. The rest of the paper is organized as follows. The model and experimental design are described in section 2. The simulation results are discussed in section 3. Conclusions and discussion are presented in the last section.

2. Model description and Experimental design

2.1 Model

The model used in this study is the WRF model, version 3.9.1. The model domain is triply nested with the three meshes of 6300 km by 6300 km, 1080 km by 1080 km, and 600 km by 600 km and their respective horizontal grid spacings of 18, 6, and 2 km, respectively. There are 47 levels in the vertical. The model physics used in this study include the single-moment 6-class cloud microphysics scheme (WSM6, Hong & Lim, 2006), the Kain-Fritsch cumulus scheme (Kain, 2004) for the outermost mesh, the Yonsei University scheme for planetary boundary layer vertical mixing (YSU, Hong et al., 2006) and the Monin-Obukhov scheme for surface stress and flux calculations (see those related to spray below), the Dudhia shortwave (Dudhia, 1989), and the Rapid Radiative Transfer Model (RRTM) longwave schemes (Mlawer et al., 1997) for radiation flux calculations.

2.2 Sea spray parameterization

The surface air-sea enthalpy flux includes two components, namely the interfacial exchange and the spray-mediated exchange (Fairall et al., 1994). The interfacial sensible and latent heat fluxes are calculated with the bulk aerodynamic scheme as following:

$$HS = \rho_a c_{pa} C_H U (T_o - T_a + \delta T_a) \tag{1}$$

147
$$HL = \rho_a L_e C_E U \left(q_s(T_o) - q_s(T_d + \delta T_d) \right) \tag{2}$$

where HS and HL are the direct interfacial sensible and latent heat fluxes, respectively; ρ_a is the surface air density of dry air; c_{pa} is specific heat of dry air at constant pressure; L_e is the latent heat of vaporization; C_H and C_E are the surface exchange coefficients for sensible heat and latent heat, respectively (often $C_H = C_E$ is assumed); U is the near-surface horizontal wind speed; T_o is the sea surface temperature; T_a is the air temperature near the ocean surface; T_d is the dewpoint temperature; T_a is the saturation mixing ratio of water vapor at temperature T_o ; δT_a and δT_d are

the changes of air temperature and dewpoint temperature due to spray feedback (Bao et al., 2011).

The spray-mediated enthalpy flux is determined by detailed spray microphysical processes, such as the size distribution, source function, and mass flux of spray droplets, etc. (Fairall et al., 1994; Andreas & Emanuel, 2001; Bao et al., 2011) and is estimated using the version 12 of Fairall et al. (1994) scheme in this study, which is downloaded from the website https://downloads.psl.noaa.gov/BLO/Air-Sea/onr_droplet/parameterization/version12. The spray-mediated heat flux due to temperature change of droplets (*QS*) is calculated as following:

$$QS = 0.92c_{pw}M_V(T_o - T_w)$$
 (3)

where 0.92 accounts for the loss of heat not transferred from the very large droplets; c_{pw} is the water specific heat; M_V is the spray mass flux; T_w is the wet bulb temperature of seawater droplet; The spray mass flux M_V with unit of $\frac{kg}{m^2 \cdot s}$ is given by

$$M_V = \zeta \rho_w p_w S_V \tag{4}$$

where ζ is a spray-source function-tuning parameter and the currently accepted value is 0.3 (Gall et al., 2008); ρ_w is the water density; p_w is the energy inputted by waves with unit of m³ s⁻³ and is estimated as follows:

$$p_w = 0.5 \times \frac{\rho_a}{\rho_w} c_w u_*^2 \tag{5}$$

where c_w is the phase speed of breaking waves and is estimated by $c_w = 0.1 + 0.23U$. u^* is the friction velocity, which satisfies $u_*^2 = C_D U^2$ with C_D being the surface drag coefficient. With different C_D schemes, the estimated friction velocities (u^*) and hence the inputted wave energies (p_w) and spray mass fluxes (M_V) are different, making the spray mediated enthalpy fluxes different. When the temperature of droplet reaches equilibrium, the temperature of droplet is the same from the inner to the surface. Hence, the mass flux associated with sensible heat transfer is estimated with the volume flux of the droplet. S_V is the normalized source function of volume with unit of

 $(m^3 \cdot \frac{1}{m^2 \cdot s})/(\frac{m}{s})^3$, being the volume of spray generated in per square meter, per second, per unit of inputted wave energy. In high-wind conditions, spray droplets are mainly formed when the wind stress tears off the crest of waves, and hence, S_V is parameterized by the characteristics of waves as

180
$$S_V = 2.9 \times 10^{-5} \left[1 + \left(\frac{h_W}{3} \right)^{0.1} \right] \left(\frac{55 \times v^{0.7} + 20}{50} \right)^{2.5}$$
 (6)

where h_w is half of the significant wave height, estimated by $h_w = (2 + 10U/60)/2$; v is the mean fall velocity of spray droplets that is positively correlated to surface wind speed and phase speed of breaking waves and negatively correlated to friction velocity.

After the temperature of droplet falls to T_w , the droplet will evaporate by absorbing sensible heat from its environment. The spray-mediated flux due to evaporation of droplets (QL) at the equilibrium state is calculated as following:

$$QL = L_e M_S [q_S (T_a - \delta T_a) - q_S (T_d + \delta T_d)] \tag{7}$$

where M_S is the spray mass flux due to evaporation. If all the droplets evaporate in the air, M_S is the same as M_V . However, this is often not true (Andreas & Emanuel, 2001). As the timescales for evaporation are large, only part of the droplet evaporates and the rest will re-enter the ocean. M_S should be different from M_V . The evaporation only takes place in the surface of droplets, therefore, M_S is estimated via surface area with unit of $\frac{kg}{m^2 \cdot s}$, which is calculated by

193
$$M_S = \zeta \rho_a p_w h_w \beta S_a \left[1 - 0.27 \left(1 + \frac{1}{1 - RH} \right) \right]^{0.33}$$
 (8)

where RH is the relative humidity of the surface air; S_a is the normalized source function of spray droplets of surface area with unit of $\left(m^2 \cdot \frac{1}{m^2 \cdot s}\right) / \left(\frac{m}{s}\right)^3$, being the surface area that spray evaporate in per square meter, per second, per unit of inputted wave energy. As the energy inputted by waves is considered to be converted to potential energy in the surface tension of droplets (Fairall et al.,

198 2009), S_a could be estimated by the inputted energy and is given by

199
$$S_a = 4.5 \times \left(\frac{p_w}{6.0 \times 10^{-4}}\right)^{0.15} \times \left(\frac{55 \times v^{0.7} + 20}{50}\right)^{-1}$$
 (9)

200 and β is the coefficient calculated by

$$\beta = \left(1 + \frac{L_e^2 q_s(T_a)}{c_{pa} R_v T_a^2}\right)^{-1} \tag{10}$$

where R_{ν} is the gas constant of water vapor.

In the presence of spray, QS computed in Eq. (3) is the enthalpy flux carried by the droplets as they are ejected from the sea surface at T_o and cool to T_w . However, only the heat transferred to the air while the droplets cool from T_o to T_a is the "sensible heat" part, which is the QS_s (Andreas and Emanuel, 2001; Ma et al., 2015). After their temperature fall from T_a to T_w , the droplets evaporate and the heat is transferred into the atmosphere via the evaporation rather than directly warming the surrounding air via "sensible heat". As a result, the remainder of QS (i.e., cooling from T_a to T_w) was allotted to "latent heat" QS_l . The total air-sea sensible heat (HS_{tot}) and latent heat (HL_{tot}) fluxes are:

$$HS_{tot} = HS + QS_s - QL \tag{11}$$

$$HL_{tot} = HL + QS_l + QL \tag{12}$$

213 where QS_s and QS_l are

$$QS_S = \frac{T_o - T_a + \delta T_a}{T_o - T_w} QS \tag{13}$$

$$QS_l = \frac{T_a - T_w - \delta T_a}{T_o - T_w} QS \tag{14}$$

216 2.3 Surface drag coefficient (C_D)

As we mentioned above the spray-mediated enthalpy flux is a function of friction velocity given in Eq. (5), which is a function of surface drag coefficient C_D . To show how the simulated TC depends on the C_D parameterization, two typical C_D schemes were used in this study, representing

the two different trends of C_D in high-wind regime (Fig. 1). One is the default scheme in the WRF model, which is based on the Monin-Obukhov similarity theory (Large & Yeager, 2009) and modified for TC simulations. C_D initially increases with increasing 10-m wind speed but is kept constant for 10-m wind speed above 30 m s⁻¹. The other scheme is that described in Donelan (2018), in which C_D decreases with 10-m wind speed in the regime between 30 and 60 m s⁻¹ and slightly increases with 10-m wind speed in the regime for wind speed above 60 m s⁻¹. Note that the aim of this study is not to validate which scheme we are testing is better, as both are commonly used in idealized and real-case TC simulations. Rather, this study is to examine the dependence of spray effect on C_D schemes in idealized simulations. Results from this study also indicate that more work is needed to validate both the C_D scheme and spray parameterization for improving TC intensity and structure forecasts using numerical models.

2.4 Experimental design

In this study, we performed idealized numerical simulations on an f-plane of 20°N. The model was initialized with an axisymmetric cyclonic vortex embedded in a quiescent and horizontally uniform environment, which has the mean tropical sounding of temperature and humidity given in Jordan (1958). The sea surface temperature was fixed at 28°C. The initial TC vortex was in hydrostatic and gradient wind balance with a maximum near-surface wind speed of 15 m s⁻¹ at a radius of 82.5 km.

Two sets of experiments (Table 1) were designed to investigate the dependence of the spray effect on the simulated TC evolution on the C_D scheme used. In WRF_CTRL, the WRF default C_D scheme was used with no spray effect included. In WRF_SPY, the WRF default C_D scheme was used with the spray effect included. In Donelan_CTRL, the Donelan C_D scheme was used with no spray effect included, while in Donelan_SPY, the Donelan C_D scheme was used with the spray

effect included.

3. Results

243

244

245

246

247

248

249

250

251

252

253

254

255

256

257

258

259

260

261

262

263

264

265

Before we discuss the effect of spray, we first briefly compare the intensity evolutions of the simulated TCs in the two experiments with different C_D schemes without inclusion of the spray effect. Figure 2 shows the time series of the maximum wind speeds at the lowest model level and the central sea level pressure simulated in WRF CTRL and Donelan CTRL. The intensity evolutions of the TCs in the two experiments are similar but with some visible differences, especially after about 40 h of simulations. After an initial 24-h spinup, the simulated TC experiences a rapid intensification stage up to about 102 h of simulations, which is followed by a slow evolving, quasi-steady intensity evolution stage. The TC simulated in Donelan CTRL is stronger than that in WRF CTRL in both the intensification and mature stages. The central sea level pressure in Donelan CTRL is about 18 hPa lower than that in WRF CTRL, and the maximum wind speed at the lowest model level is about 24 m s⁻¹ higher by 199 h of the simulations. This is consistent with what is expected from the maximum potential intensity (MPI) theory (Emanuel, 1986, 1995), which implies that the maximum TC intensity is inversely proportional to the square root of C_D. Since the spray-mediated flux depends on surface wind speed, it is expected that the effect of the parameterized spray on TC structure and intensity may vary with TC intensity or different stages of the TC development. Therefore, in the following discussion, we will discuss the spray effects on the simulated TC in the intensification stage and the mature stage, separately.

3.1 Primary intensification stage

Figure 3 compares the intensity evolutions of the simulated TCs in experiments with and without sea spray effect using the two different C_D schemes. During the primary intensification stage (60–102 h), the TC in WRF SPY is stronger than that in WRF CTRL and the difference

between the maximum surface wind speed reaches 11 m s⁻¹. In the experiments with the WRF C_D scheme, the TC with the spray effect is stronger (Fig. 3a), which is consistent with previous studies (Wang et al., 2001; Ma et al., 2015). However, in the same time period, the TC with the spray effect is weaker than that without the spray effect with the Donelan C_D scheme (Fig. 3b), which is in contrast to that with the WRF C_D scheme. This indicates that the spray effect on TC intensity evolution depends on the surface drag scheme used in the numerical model.

266

267

268

269

270

271

272

273

274

275

276

277

278

279

280

281

282

283

284

285

286

287

288

The spray-mediated sensible and latent heat fluxes averaged in the primary intensification stage of 60–102 h in the two spray experiments with different C_D schemes are shown in Fig. 4. The radial distribution of the spray-mediated sensible heat flux is comparable with that shown in previous studies (Gall et al., 2008; Ma et al., 2015). The peak values are located under the eyewall, while the lowest (negative) values are outside the eyewall about 75 km away from the TC center with negative values of -10.0 and -15.5 w m⁻², respectively, in WRF SPY and Donelan SPY (Figs. 4a). This can be explained by the spray involved processes. Spray droplets with the sea surface temperature, which is warmer than the boundary layer air temperature, release sensible heat to the air. This sensible heat is determined by the air-sea temperature difference and the quantity of spray mass flux mainly controlled by the wind stress. In the meantime, evaporation of spray droplets absorbs sensible heat from the environment, which is mainly controlled by the relative humidity of the surrounding air (Fairall et al., 1994). Under the TC eyewall with high wind speed, spray droplets release large sensible heat due to high air-sea temperature difference but absorb relatively little sensible heat due to evaporation because the air is nearly saturated. This results in the peak value of the spray-mediated sensible heat under the eyewall. In the region outside the eyewall, less sensible heat is released by spray droplets because of less spray droplets generated under relatively weak wind speed and smaller air-sea temperature difference. In addition, the relative humidity often

decreases rapidly outside the eyewall. As a result, a considerable percentage of spray droplets evaporate, absorbing large amount of sensible heat from the environmental air and leading to negative net sensible heat flux outside of the eyewall. However, due to evaporation during their lifetime suspended in the air, spray-meditated latent heat flux is positive at all radii (Figs. 4b). Although less percentage of droplets evaporate in the eyewall region, a plenty of droplets are generated due to high wind speed, and thus the overall latent heat flux was still the greatest under the eyewall region.

289

290

291

292

293

294

295

296

297

298

299

300

301

302

303

304

305

306

307

308

309

310

311

It is the surface latent heat flux that dominate the energy supply for the development and maintenance of a TC. Therefore, we compare the total surface latent heat fluxes in different experiments to examine how the inclusion of sea spray may modify the total latent flux. Figure 5 shows the difference in the azimuthal-mean total latent flux between the runs with and without the spray effect included. During the intensification stage in experiments with the WRF C_D scheme, the surface latent heat flux in WRF SPY is greater inside the radius of maximum wind (RMW) than that in WRF CTRL, while is mostly smaller outside the RMW (Fig. 5a). In contrast, during the 60–102 h, the surface latent flux is generally smaller inside the RMW and greater outside the RMW in Donelan SPY than in Donelan CTRL (Fig. 5b). The simulated TC intensified with a relatively greater intensification rate in the case with greater surface latent heat flux inside the RMW (Table 1), which is consistent with the findings of Xu & Wang (2010) and Wang & Heng (2016). They found that surface flux near and inside the RMW is favorable for TC intensification, while that beyond a radius of 2-3 times of the RMW is unfavorable for TC intensification, but important to the inner-core size growth. They showed that the radial distribution and magnitude of surface latent heat flux affects the strength and radial location of convection and thus the TC intensification. As we can see from Fig. 6, with the sea spray effects included, during the primary

intensification stage (60–102 h), the surface latent heat flux and upward motion (and thus convection) in WRF_SPY increased inside the RMW but decreased outside the RMW (Fig. 6a), making the TC stronger than that in WRF_CTRL. In contrast, the surface latent heat flux and convection in Donelan_SPY decreased inside the RMW and increased outside the RMW (Fig. 6b), resulting in the weaker TC than that in Donelan_CTRL.

312

313

314

315

316

317

318

319

320

321

322

323

324

325

326

327

328

329

330

331

332

333

334

The difference in the radial distribution of surface latent heat flux in different C_D experiments results primarily from the dependence of the spray mass flux on sea surface wind stress, which depends on C_D. During 60–102 h, the wind speed around the RMW exceeds 30 m s⁻¹, and thus C_D is constant with the WRF C_D scheme, while the wind speed and thus C_D is smaller in the outer region than in the inner core. As a result, in the experiment with the WRF scheme, C_D is maximum around the RMW (Fig. 7). This leads to large spray mass flux and thus spray-mediated latent heat flux around the RMW in WRF SPY (Fig. 8), which is beneficial for the TC intensification. In contrast, in the experiments with the Donelan C_D scheme, after 60 h of simulation, the wind speed in the inner core in both Donelan CTRL and Donelan SPY increase gradually and exceeds 30 m s⁻¹, indicating that C_D in the inner core would decrease with TC intensification. At the same time, the wind speed in the outer region is weaker than 30 m s⁻¹, C_D increases with TC intensification and is even larger than that in the inner core (Fig. 7). The maximum value C_D averaged during 60– 102 h occurs near the radius of 60 km from the TC center, producing relatively large spray-mediated latent heat flux in this region (Fig. 8). The increased spray-mediated latent flux in the outer region is not beneficial for TC intensification.

It can be seen from Fig. 4 that the spray-mediated latent flux is generally smaller than 50 W m⁻² during the primary intensification stage. However, the difference in latent flux between spray experiment and control experiment is even larger and could be over 100 W m⁻² (Fig. 5), leading to

considerable difference in TC intensification rate (Fig. 3). This suggests that other processes associated with the C_D scheme may make positive feedback between spray and TC intensity. Many studies have shown that the response of boundary layer dynamics to C_D is a fast process and plays a significant role in affecting TC intensification (Kepert and Wang, 2001; Kepert 2017). Li & Wang (2021a, b) found that C_D induced boundary layer inflow can determine the strength and radial location of mass convergence and eyewall updraft. A larger CD, thus greater surface friction, corresponds to greater moisture convergence, providing faster moistening and organization of convection. This contributes to the different effects of spray when the different C_D schemes are used. During 60–102 h of the simulation with the WRF C_D scheme, C_D is maximum around the RMW (Fig. 7), which is beneficial for the inward penetration of spray-mediated latent heat into the inner core region. This leads to greater total latent heat flux and convection around the RMW (Fig. 5a, Fig. 6a), making the stronger TC in WRF SPY. However, in the experiments with the Donelan C_D scheme, C_D is maximum outside the RMW (Fig. 7). This is beneficial for the moisture convergence and spray mass flux at those radii. Smaller C_D near the RMW of 28 km is unfavorable for the inward penetration of boundary layer inflow, giving rise to a tendency of increasing mass and moisture convergence between the radii 28 km and 60 km. Furthermore, smaller C_D is unfavorable for spray mass flux near the RMW. Compared with Donelan_CTRL, considerable spray-mediated latent heat flux, and thus convection, in Donelan SPY is located slightly outside of the RMW (Fig. 8b and Fig. 6b), which slows down the intensification rate of the simulated TC in Donelan SPY (Fig. 3b, Table 1). From Figs. 9c, d and Table 1, we also can see that the size of the simulated TC in Donelan SPY expands outward relative to that in Donelan CTRL. This is consistent with the finding in Xu & Wang (2010).

335

336

337

338

339

340

341

342

343

344

345

346

347

348

349

350

351

352

353

354

355

356

357

Figure 10 compares the radius-height distributions of the azimuthal-mean radial wind, vertical

motion, and inertial stability between experiments with and without spray effects. As a result of the higher intensity of the TC in WRF SPY, the radial inflow under the eyewall is about 1.9 m s⁻¹ (11%) stronger than that in WRF CTRL, and the maximum upward motion in the eyewall is enhanced by about 0.6 m s⁻¹ (35%). The inertial stability is also enhanced, which implied relatively more rapid intensification rate of the TC because higher inner-core inertial stability indicates higher efficiency of eyewall heating in spinning up tangential wind near the RMW (Schubert & Hack, 1982; Pendergrass & Willoughby, 2009). Consistent with the weaker TC in Donelan SPY, both the radial inflow and upward motion are weaker (-10% and -8% respectively) between the radii of 25 and 50 km than those in Donelan CTRL. However, there is an increase in radial inflow and upward motion outside the eyewall between the radii of 60 and 90 km in Donelan SPY, indicating less penetrative of the boundary layer inflow into the eyewall region. This might be due to the larger C_D outside the RMW, which induces more spray-mediated latent heat flux, promotes boundary layer moisture and mass convergence, and hence enhances upward motion relative to those in Donelan CTRL. As a result of the stronger moisture convergence and convection in the region outside the RMW, the wind and hence the inertial stability are also enhanced as shown in Fig. 10f. The increased inertial stability outside the RMW in turn may impedes inflow toward the eyewall region, partially suppressing TC intensification in Donelan SPY. This is because relatively larger inertial stability outside the RMW has a greater resistance to the boundary layer inflow and thus inhabits the intensification of the TC. Therefore, in addition to the difference in the radial distribution of spray-mediated latent heat flux, the feedback from inertial stability may also partly contribute to the different intensification rates of the simulated TC with spray effects using different C_D schemes.

358

359

360

361

362

363

364

365

366

367

368

369

370

371

372

373

374

375

376

377

378

379

380

The above analysis indicates that during the primary intensification stage, because CD is

greater outside the RMW than that near the RMW with the Donelan C_D scheme, the larger spray-mediated latent heat flux and stronger moisture convergence outside the RMW result in enhanced convection outside the RMW and reduced intensification rate of the simulated TC relative to the TC simulated without spray effect. In the meantime, the increased inflow outside the RMW also leads to the increase in the local tangential wind and the inertial stability, which in turn can further reduce the inward penetration of inflow into the eyewall region. This would also reduce the intensification rate of the simulated TC. The opposite conditions apply to the simulations with the WRF C_D scheme, leading to the more rapid intensification for the TC with spray effect than in the simulation without the spray effect included.

3.2 Mature stage

Although the TC is not necessarily stronger after incorporating spray during the primary intensification stage, the intensity of the TC with spray effect is consistently greater at mature stage (144-192 h) than that without the spray effect (Fig. 3). The maximum TC intensities during the mature stage in WRF_SPY and Donelan_SPY increase by 12% and 7%, respectively, relative to their corresponding intensities in WRF_CTRL and Donelan CTRL. The greater final intensity of the simulated TC with spray effect is consistent with the MPI theory, which predicts a proportion of the maximum wind speed of the TC to the square root of C_E/C_D under the eyewall. Spray droplets are injected into the air with the sea surface temperature, and some of which fall back into the sea with the equilibrium temperature with the air. That means during suspending in the air, the spray droplets release an appreciable sea-air enthalpy flux and act as a heating source of the TC boundary layer, being comparable with a larger C_E . We can see from Fig. 11 that at mature stage the boundary layer inflow, the eyewall convection and inertial stability in WRF_SPY and Donelan_SPY are all enhanced in the inner-core region, compared with the corresponding variables in WRF_CTRL and

Donelan CTRL, corresponding to the stronger TCs in the simulations with the sea spay effects.

404

405

406

407

408

409

410

411

412

413

414

415

416

417

418

419

420

421

422

423

424

425

426

At mature stage in WRF SPY, the wind speed outside the eyewall exceeds 30 m s⁻¹, and hence C_D near the RMW and in the near-core environment are almost equal (Fig. 11). This indicates considerable spray mass flux and thus spray-mediated latent heat flux both near and outside the RMW. The increased latent heat flux outside the RMW due to spray evaporation is favorable for convective activity outside the eyewall. As we can see from Fig. 11, compared with that in WRF CTRL, the inflow in WRF SPY shows a larger local maximum in the boundary layer and larger weak outflow above (Fig. 11a) with stronger upward motion between the radii of 60–100 km (Fig. 11b). This implies more active spiral rainbands in the region. The enhanced inflow favors the spinup of tangential wind and thus increase in inertial stability in the region (Fig. 11c). The increased inertial stability favors the increase in boundary layer inflow in the outer core region. Such an effect is beneficial to the outward expansion of both inflow and tangential wind and thus the increase in the inner-core size of the simulated TC, as evident in Figs. 9a, b. As a result, in addition to the higher TC intensity in experiment with spray effect using the WRF C_D scheme than in the control experiment without considering the spray effect, the change of the TC size (RHW, radii of hurricane force wind, $\geq 32.7 \text{ m s}^{-1}$) at the mature stage is also considerably larger (Fig. 9, Table 1).

The radial distribution of C_D in the simulation with the Donelan scheme at the mature stage shows a different distribution from that with the WRF scheme (Figs. 11a, d). Now C_D peaks in the outer core region, relatively far away from the RMW at mature stage as inferred from the wind speed dependence of C_D shown in Fig. 1. The larger C_D produces higher spray mass flux in Donelan_SPY, and thus larger spray-mediated latent heat flux in the outer region beyond the radius of 100 km from the TC center. In the region near the RMW, C_D is larger inside the RMW and lower

outside the RMW (Fig. 11d). This leads to the increased spray mass flux and thus spray-mediated latent heat flux inside the RMW but relative smaller spray-mediated latent heat flux outside the RMW in the inner-core region within a radius of 90 km (Fig. 8b). This is unfavorable for the outward expansion of tangential wind and the increase in the inner-core size of the simulated TC (Xu & Wang, 2010). Although the increased C_D is also evident outside a radius of 100 km from the TC center, the wind speed is often weaker and thus the spray-mediated latent heat flux becomes relatively small with no evidence of any enhanced convective activity in the outer-core region compared to the experiment without the spray effect included (Fig. 11e). This is also consistent with the lack of any obvious outward expansion of the TC size compared with that in the simulation in Donelan CTRL (Figs. 9c, d).

4. Summary and Discussion

The dependence of the sea spray effects on TC evolution on the surface drag coefficient parameterization is investigated with two different C_D schemes using the WRF model. The first C_D scheme is the one commonly used for TC simulations/predictions in the WRF model, namely C_D increases linearly with 10-m wind speed in the low-wind regime (less than 30 m s⁻¹) and is a constant when wind speed is above 30 m s⁻¹. The second C_D scheme is the one recently developed by Donelan (2018), which is obtained based on laboratory experiments. In the Donelan scheme, C_D increases with increasing 10-m wind speed in the low-wind regime (less than 30 m s⁻¹) and decreases with increasing 10-m wind speed when 10-m wind speed between 30 m s⁻¹ and 60 m s⁻¹, and slightly increases again afterwards. The Version 12 of the Fairall spray scheme (1994) is used to parameterize the spray processes.

In the experiments with the sea spray effect, the spray-mediated sensible heat flux is positive inside the RMW and negative outside the RMW. Spray droplets release sensible heat due to the

temperature difference between the initial droplet temperature and the surrounding air temperature. On the other hand, the evaporation of spray droplets absorbs sensible heat from the surrounding air. In the inner-core region, only a small portion of spray mass evaporates, and hence the net sensible heat flux is positive. However, in the outer region, higher proportion of mass evaporates and the sensible heat released by spray droplets cannot offset the sensible heat absorbed by evaporation. As spray droplets evaporate at all radii, the spray-mediated latent heat flux is always positive. As a result, for a mature TC, the additional spray-mediated latent heat may result in an increase in the total surface enthalpy flux, which can lead to an increase in the maximum TC intensity, as predicted by the MPI theory. This explains why the simulated TCs at the mature stage are stronger in the experiments with the spray effects included than those in the corresponding experiments without spray effects regardless which surface drag coefficient scheme is used.

However, during the primary intensification stage, sea spray may either enhance or reduce the intensification rate of the simulated TC depending on the C_D scheme used (Fig.3, Table 1). This is because the different dependence of C_D on near-surface wind speed can result in spray mass flux, which depends on the near-surface wind speed. Such a dependence can lead to the difference in the radial distribution of C_D , and thus the spray mass flux and the spray-mediated latent heat flux. In the Donelan scheme, C_D is maximum outside the RMW, which produces relatively large spray-mediated latent heat flux well outside the RMW. The larger C_D outside the RMW is also unfavorable for the inward penetration of the spray-mediated latent heat, giving rise to a tendency of increasing mass and moisture convergence outside the RMW and thus the reduced intensification rate compared to the experiment without the spray effects included. On the contrary, in the WRF default scheme, C_D is a constant when the near-surface wind speed is over 30 m s⁻¹ and is greater near the RMW. This leads to large spray mass flux and thus the spray-mediated latent heat flux

around the RMW. The larger C_D around the RMW is also beneficial for the inward penetration of spray-mediated latent heat. As a result, the intensification rate of the TC simulated with the spray effects is larger than that without the spray effects included in the WRF C_D scheme (Fig.3, Table 1).

473

474

475

476

477

478

479

480

481

482

483

484

485

486

487

488

489

490

491

492

493

494

495

Sea spray also affects the inner-core size change of the simulated TC. This is because sea spray can modify the radial distribution of latent heat flux, depending on the spray mass flux, which is a function of surface wind stress partly affected by the wind speed dependence of C_D. When C_D is greater near the RMW, more spray droplets would be generated under the eyewall and thus enhances surface latent heat flux, and larger C_D is also beneficial for the inward penetration of spray-mediated latent heat into the RMW. These may contribute to the contraction of the RMW of the TC and hence insignificant outward expansion of the TC inner-core size, such as in the primary intensification stage in WRF SPY and in the mature stage in Donelan SPY. However, during the primary intensification stage in Donelan SPY and the mature stage in WRF SPY, CD is relatively greater outside the RMW. This produces considerable sea spray mass flux and the associated spraymediated latent heat flux, contributing to the enhanced boundary layer inflow spinning up of tangential wind and the increase in inertial stability outside the eyewall. The positive feedback between the inertial stability and the outward expansion of tangential wind further enhances convection outside the eyewall. This would lead to the inner-core size increase. This is more pronounced during the later intensification stage and during the mature stage in WRF SPY. Therefore, our results suggest that different C_D schemes can induce difference in the radial distribution of sea spray mass flux and spray-mediated latent heat flux and thus the size change of TCs, in support the findings of Xu & Wang (2010). The detailed effects, however, may differ during different stages of TC development because C_D often depends on near-surface wind speed and thus

the TC intensity.

Results from this study also indicate that in addition to how much sea spray is generated and its mediated enthalpy flux, the radial distribution resulting from the dependence of sea spray mass flux on surface wind stress and thus surface drag coefficient scheme is also important when the effect of sea spray on TC evolution is incorporated in numerical models used for simulating and predicting TCs. Indeed, the simulated TC intensity and size change in response to the sea spray effects differ during different stages of the TC development, which is shown to result from the different dependence of surface drag coefficient on near-surface wind speed. Therefore, our results demonstrate that caution needs to be given to the surface drag parameterization when the sea spray effects on TC evolution is studied and discussed using numerical sensitivity experiments. Note that in addition to the surface drag coefficient, the TC structure and environmental conditions may also modify the radial distribution of spray mass flux and the related spray-mediated enthalpy flux under TC conditions. These needs to be further investigated in future work.

Finally, it should be pointed out that in this study we have only considered the direct effect of sea spray caused by using different C_D schemes, which only control the energy inputted by breaking waves through Eq. (5) and thus the spray mass flux through Eq. (4). In addition to C_D, spray mass flux is also largely controlled by the properties of the breaking waves. In the sea spray parameterization we used, both the significant wave height and the phase speed of breaking waves are parameterized as a function of wind speed, which is independent of C_D. This means that the possible coupling between C_D and breaking waves is not included in the current spray parameterization. In this sense, in terms of the sensitivity of spray effect on the simulated TCs to C_D is incomplete. To fully address the issue, a coupled ocean-atmosphere-wave-spray model should be developed and used. This can be a topic for a future study. Nevertheless, results from this study

have demonstrated the importance of C_D scheme to the parameterized spray effect on the simulated TC evolution. Large uncertainties exist in the parameterized sea spray source function and spray properties, including the spray size distribution. Therefore, efforts to measure spray properties under TC conditions should be conducted to provide data for validation and improvements of current spray parameterization scheme in future studies. **Acknowledgments**: The authors are grateful to two anonymous reviewers for their constructive review comments, which helped improve the manuscript. This study was supported in part by the National Key R&D Program of China under grants (2017YFC1501602, 2018YFB1501104 and 2021YFC3000803), the National Natural Science Foundation of China under grants (41806046, 41730960, 41775064), Program of Shanghai Academic/Technology Research Leader (21XD1404500), S&T Development Fund of STI (2022KJFZ04), and in part by the Scientific Research Program of Shanghai Science and Technology Commission under grant (19dz1200101). YW was partly supported by NSF grant AGS-1834300.

519

520

521

522

523

524

525

526

527

528

529

530

531

532

533

534

535

Data availability: Initial conditions and model configuration files are publicly available from Duan (2022). The version 12 spray parameterization of Fairall et al. (1994) scheme used in this study is downloaded from the website https://downloads.psl.noaa.gov/BLO/Air-Sea/onr droplet/parameterization/version12.

536 **References:**

- Andreas, E. L. (1992). Sea spray and the turbulent air-sea heat fluxes. Journal of Geophysical
- 538 Research: Oceans, 97(C7), 11429-11441. https://doi.org/10.1029/92JC00876
- Andreas, E. L., & Emanuel, K. A. (2001). Effects of sea spray on tropical cyclone intensity. *Journal*
- 540 of the Atmospheric Sciences, 58(24), 3741-3751. https://doi.org/10.1175/1520-
- 541 0469(2001)058<3741:EOSSOT>2.0.CO;2
- Bao, J., Fairall, C. W., Michelson, S. A., & Bianco, L. (2011). Parameterizations of sea-spray
- impact on the air—sea momentum and heat fluxes. *Monthly Weather Review*, 139(12), 3781-3797.
- 544 https://doi.org/10.1175/MWR-D-11-00007.1
- Black, P. G., D'Asaro, E. A., Drennan, W. M., French, J. R., Niiler, P. P., & Sanford, T. B., et al.
- 546 (2007). Air–sea exchange in hurricanes: Synthesis of observations from the coupled boundary
- layer air—sea transfer experiment. Bulletin of the American Meteorological Society, 88(3), 357-
- 548 374. https://doi.org/10.1175/BAMS-88-3-357
- Chen, S.-S., Zhao, W., Donelan, M. A., & Tolman, H. L. (2013). Directional wind-wave coupling
- in fully coupled atmosphere–wave–ocean models: Results from CBLAST-Hurricane. *Journal of*
- the Atmospheric Sciences, 70(10), 3198–3215, https://doi.org/10.1175/JAS-D-12-0157.1
- 552 Craig, G. C., Gray, S. L. (1996). CISK or WISHE as the mechanism for tropical cyclone
- intensification. Journal of the Atmospheric Sciences, 53(23), 3528-3540,
- https://doi.org/10.1175/1520-0469(1996)053<3528:COWATM>2.0.CO2
- Donelan, M. A. (2018). On the decrease of the oceanic drag coefficient in high winds. *Journal of*
- Geophysical Research: Oceans, 123(2), 1485-1501. https://doi.org/10.1002/2017JC013394
- 557 Duan, Z. (2022). WRF files for "Effects of sea spray on the simulated tropical cyclone development:
- Dependence on surface drag coefficient parameterization". [Dataset]. NJU.
- 559 https://box.nju.edu.cn/d/9b7f865aa5104111b05d/
- Dudhia, J. (1989). Numerical study of convection observed during the winter monsoon experiment
- using a mesoscale two-dimensional model. *Journal of the Atmospheric Sciences*, 46(20), 3077-
- 562 3107. https://doi.org/10.1175/1520-0469(1989)046<3077:NSOCOD>2.0.CO;2

- Edson, J. B., Anquetin, S., Mestayer, P. G., & Sini, J. F. (1996). Spray droplet modeling: 2. An
- interactive Eulerian-Lagrangian model of evaporating spray droplets. Journal of Geophysical
- 565 Research: Oceans, 101(C1), 1279-1293. https://doi.org/10.1029/95JC03280
- Emanuel, K. A. (1986). An air-sea interaction theory for tropical cyclones. Part I: Steady-state
- maintenance. Journal of the Atmospheric Sciences, 43(6), 585-605.
- 568 https://doi.org/10.1175/1520-0469(1986)043<0585:AASITF>2.0.CO;2
- Emanuel, K. A. (1995). Sensitivity of tropical cyclones to surface exchange coefficients and a
- revised steady-state model incorporating eye dynamics. Journal of the Atmospheric Sciences,
- 571 52(22), 3969-3976. https://doi.org/10.1175/1520-0469(1995)052<3969:SOTCTS>2.0.CO;2
- Fairall, C. W., Banner, M. L., Peirson, W. L., Asher, W., & Morison R. P. (2009). Investigation of
- 573 the physical scaling of sea spray spume droplet production, *Journal of Geophysical Research*,
- 574 *114*(C10), 1-19. doi:10.1029/2008JC004918
- Fairall, C. W., Kepert, J. D., & Holland, G. J. (1994). The effect of sea spray on surface energy
- transports over the ocean. Global Atmosphere and Ocean System, 2(2-3), 121-142.
- 677 Gall, J. S., Frank, W. M., & Kwon, Y. (2008). Effects of sea spray on tropical cyclones simulated
- under idealized conditions. Monthly Weather Review, 136(5), 1686-1705.
- 579 https://doi.org/10.1175/2007MWR2183.1
- Hong, S., Noh, Y., & Dudhia, J. (2006). A new vertical diffusion package with an explicit treatment
- of entrainment processes. Monthly Weather Review, 134(9), 2318-2341.
- 582 https://doi.org/10.1175/MWR3199.1
- Hong, S., & Lim, J. J. (2006). The WRF single-moment 6-class microphysics scheme (WSM6).
- *Asia-Pacific Journal of the Atmospheric Sciences*, 42(2), 129-151.
- Jordan, C. L. (1958). Mean soundings for the West Indies area. *Journal of the Atmospheric Sciences*,
- 586 *15*(1), 91-97. https://doi.org/10.1175/1520-0469(1958)015<0091:MSFTWI>2.0.CO;2
- Kain, J. S. (2004). The Kain–Fritsch convective parameterization: an update. *Journal of applied*
- 588 *meteorology*, 43(1), 170-181. https://doi.org/10.1175/1520-
- 589 0450(2004)043<0170:TKCPAU>2.0.CO;2

- Kepert, J. D. (2017). Time and space scales in the tropical cyclone boundary layer, and the location
- of the eyewall updraft. Journal of the Atmospheric Sciences, 74(10), 3305-3323,
- 592 https://doi.org/10.1175/JAS-D-17-0077.1.
- Kepert, J. D., & Wang, Y. (2001). The dynamics of boundary layer jets within the tropical cyclone
- core. Part II: Nonlinear enhancement. *Journal of the Atmospheric Sciences*, 58(17), 2485–2501,
- 595 https://doi.org/10.1175/1520-0469(2001)058<2485:TDOBLJ>2.0.CO;2.
- Kepert, J. D., Fairall, C., & Bao, J. (1999). Modelling the interaction between the atmospheric
- boundary layer and evaporating sea spray droplets. In Geernaert G. L. (Ed.), Air-sea exchange:
- Physics, chemistry and dynamics, (pp. 363-409). Dordrecht, Netherlands: Kluwer.
- Kilroy, G., Montgomery, M. T., & Smith, R. K. (2017), The role of boundary-layer friction on
- 600 tropical cyclogenesis and subsequent intensification. Quarterly Journal of the Royal
- 601 *Meteorological Society, 143*(707), 2524–2536, https://doi.org/10.1002/qj.3104
- Large, W., & Yeager, S. G. (2009). The global climatology of an interannually varying air—sea flux
- data set. Climate Dynamics, 33(2), 341-364. https://doi.org/10.1007/s00382-008-0441-3
- 604 Li, T.-H., & Wang, Y. (2021a). The role of boundary layer dynamics in tropical cyclone
- 605 intensification. Part I: Sensitivity to surface drag coefficient. Journal of the Meteorological
- Society of Japan. Ser. II, 99(2), 537-554. https://doi.org/10.2151/jmsj.2021-027
- 607 Li, T.-H., & Wang, Y. (2021b). The role of boundary layer dynamics in tropical cyclone
- 608 intensification. Part II: Sensitivity to initial vortex structure. Journal of the Meteorological
- Society of Japan. Ser. II, 99(2), 555-572. https://doi.org/10.2151/jmsj.2021-028
- Ma, Z., Fei, J., Cheng, X., Wang, Y., & Huang, X. (2015). Contributions of surface sensible heat
- fluxes to tropical cyclone. Part II: The sea spray processes. *Journal of the Atmospheric Sciences*,
- 612 72(11), 4218-4236. https://doi.org/10.1175/JAS-D-15-0058.1
- Makin, V. K. (2005). A note on the drag of the sea surface at hurricane winds. *Boundary-Layer*
- 614 *Meteorology*, 115(1), 169-176. https://doi.org/10.1007/s10546-004-3647-x
- Mestayer, P., & Lefauconnier, C. (1988). Spray droplet generation, transport, and evaporation in a
- wind wave tunnel during the Humidity Exchange over the Sea Experiments in the Simulation

- Tunnel. Journal of Geophysical Research: Oceans, 93(C1), 572-586.
- 618 https://doi.org/10.1029/JC093iC01p00572
- Mlawer, E. J., Taubman, S. J., Brown, P. D., Iacono, M. J., & Clough, S. A. (1997). Radiative
- transfer for inhomogeneous atmospheres: RRTM, a validated correlated-k model for the
- longwave. Journal of Geophysical Research: Atmospheres, 102(D14), 16663-16682.
- 622 https://doi.org/10.1029/97JD00237
- Montgomery, M. T., Smith, R. K., & Nguyen, S. V. (2010). Sensitivity of tropical-cyclone models
- 624 to the surface drag coefficient. Quarterly Journal of the Royal Meteorological Society, 136(653),
- 625 1945-1953. https://doi.org/10.1002/qj.702
- Mueller, J. A., & Veron, F. (2014a). Impact of sea spray on air-sea fluxes. Part I: Results from
- stochastic simulations of sea spray drops over the ocean. Journal of Physical Oceanography,
- 628 44(11), 2817-2834. https://doi.org/10.1175/JPO-D-13-0245.1
- Mueller, J. A., & Veron, F. (2014b). Impact of sea spray on air—sea fluxes. Part II: Feedback effects.
- 630 Journal of Physical Oceanography, 44(11), 2835-2853. https://doi.org/10.1175/JPO-D-13-
- 631 0246.1
- Pendergrass, A. G., & Willoughby, H. E. (2009). Diabatically induced secondary flows in tropical
- 633 cyclones. Part I: Quasi-steady forcing. Monthly Weather Review, 137(3), 805-821.
- 634 https://doi.org/10.1175/2008MWR2657.1
- Peng, K., Rotunno, R., & Bryan, G. H. (2018). Evaluation of a time-dependent model for the
- intensification of tropical cyclones. *Journal of the Atmospheric Sciences*, 75(6), 2125-2138.
- 637 https://doi.org/10.1175/JAS-D-17-0382.1
- Perrie, W., Zhang, W., Andreas, E. L., Li, W., Gyakum, J., & McTaggart-Cowan, R. (2005). Sea
- spray impacts on intensifying midlatitude cyclones. *Journal of the Atmospheric Sciences*, 62(6),
- 640 1867-1883. https://doi.org/10.1175/JAS3436.1
- Powell, M. D., Vickery, P. J., & Reinhold, T. A. (2003). Reduced drag coefficient for high wind
- speeds in tropical cyclones. *Nature*, 422(6929), 279-283. https://doi.org/10.1038/nature01481
- Richter, D. H., Wainwright, C., Stern, D. P., Bryan, G. H., & Chavas, D. (2021). Potential low bias

- in high-wind drag coefficient inferred from dropsonde data in hurricanes. Journal of the
- 645 Atmospheric Sciences, 78(7), 2339-2352. https://doi.org/10.1175/jas-d-20-0390.1
- Rosenthal, S. L. (1971). The response of a tropical cyclone model to variations in boundary layer
- parameters, initial conditions, lateral boundary conditions, and domain size. *Monthly Weather*
- 648 Review, 99(10), 767-777. https://doi.org/10.1175/1520-
- 0493(1971)099<0767:TROATC>2.3.CO;2
- Rouault, M. P., Mestayer, P. G., & Schiestel, R. (1991). A model of evaporating spray droplet
- dispersion. Journal of Geophysical Research: Oceans, 96(C4), 7181-7200.
- 652 https://doi.org/10.1029/90JC02569
- 653 Schubert, W. H., & Hack, J. J. (1982). Inertial stability and tropical cyclone development. *Journal*
- of the Atmospheric Sciences, 39(8), 1687-1697. https://doi.org/10.1175/1520-
- 655 0469(1982)039<1687:ISATCD>2.0.CO;2
- 656 Thomsen, G. L., Montgomery, M. T., & Smith, R. K. (2012). Sensitivity of tropical-cyclone
- intensification to perturbations in the surface drag coefficient. Quarterly Journal of the Royal
- 658 *Meteorological Society*, 140(679), 407–415. https://doi.org/10.1002/qj.2048
- Wang, Y., Kepert, J. D., & Holland, G. J. (2001). The effect of sea spray evaporation on tropical
- 660 cyclone boundary layer structure and intensity. *Monthly Weather Review*, 129(10), 2481-2500.
- https://doi.org/10.1175/1520-0493(2001)129<2481:TEOSSE>2.0.CO;2
- Wang, Y., & Heng, J. (2016). Contribution of eye excess energy to the intensification rate of
- tropical cyclones: A numerical study. Journal of Advances in Modeling Earth Systems, 8(4),
- 1953-1968. https://doi.org/10.1002/2016MS000709
- Wang, Y., Li, Y.-L., Xu, J., Tan, Z.-M., & Lin, Y.-L. (2021a). The intensity-dependence of tropical
- 666 cyclone intensification rate in a simplified energetically based dynamical system model. *Journal*
- of the Atmospheric Sciences, 78(7), 2033–2045, https://doi.org/10.1175/JAS-D-20-0393.1
- Wang, Y., Li, Y.-L., & Xu, J. (2021b). A new time-dependent theory of tropical cyclone
- intensification. Journal of the Atmospheric Sciences, 78(12), 3855–3865,
- 670 https://doi.org/10.1175/JAS-D-21-0169.1

- Wang, Y., Tan, Z.-M., Li, Y.-L. (2022). Some refinements to the most recent simple time-dependent
- theory of tropical cyclone intensification and sensitivity. *Journal of the Atmospheric Sciences*,
- 673 79, https://doi.org/10.1175/JAS-D-22-0135.1
- Ku, J., & Wang, Y. (2010). Sensitivity of tropical cyclone inner-core size and intensity to the radial
- distribution of surface entropy flux. Journal of the Atmospheric Sciences, 67(6), 1831-1852.
- 676 https://doi.org/10.1175/2010JAS3387.1

List of Tables

Table 1. Summary of the numerical experiments performed in this study, the mean intensification rate (IR, m s⁻¹ h⁻¹) during the primary intensification stage (60–102h), the steady-state (144–192h) mean intensity, and the stage-means of the size parameters (RMW–the radius of maximum wind and Δ RHW–change of the radius of hurricane force wind).

	C_D	Spray	60-102 h			144-192 h		
	scheme		IR (m s ⁻¹ h ⁻¹)	RMW (km)	ΔRHW (km h ⁻¹)	Intensity (m s ⁻¹)	RMW (km)	ΔRHW (km h ⁻¹)
WRF_CTRL	WRF	No	0.47	30.7	0.66	56.0	47.2	0.72
WRF_SPY	WRF	Yes	0.54	27.5	0.48	63.0	42.9	0.94
Donelan_CTRL	Donelan	No	0.62	28.1	0.54	66.7	44.0	0.57
Donelan_SPY	Donelan	Yes	0.57	29.2	0.59	75.1	38.5	0.37

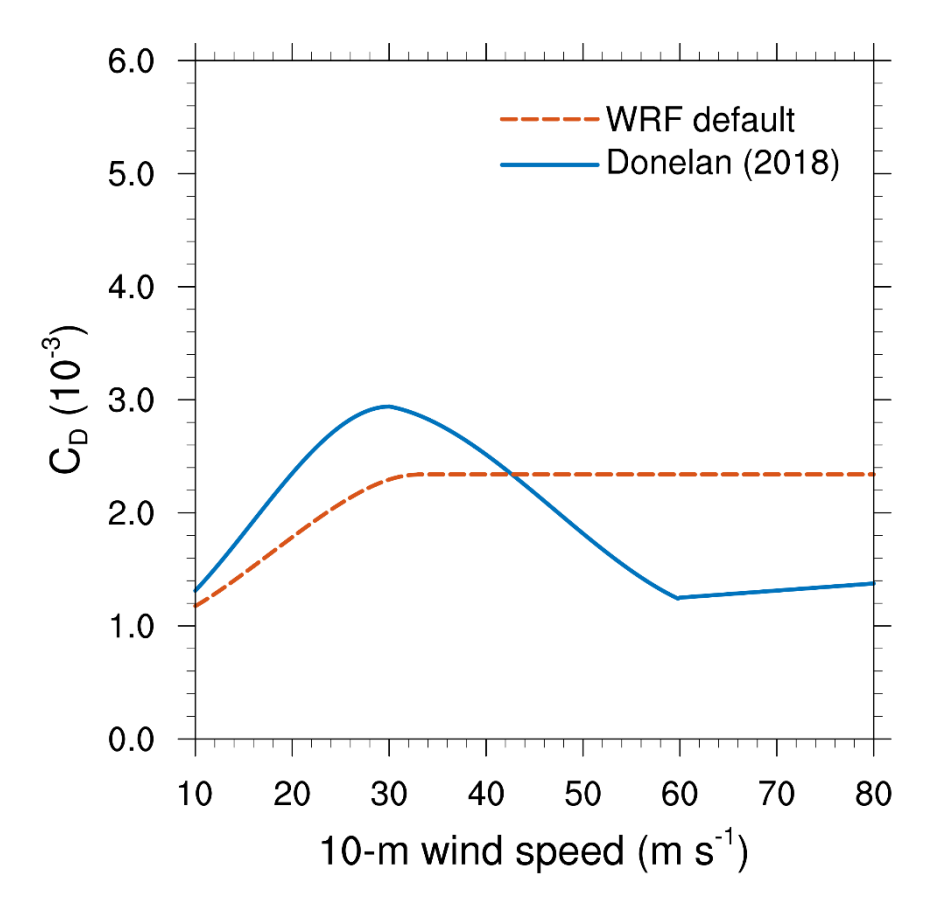


Figure 1. The dependence of surface drag coefficient (C_D) on surface wind speed for the default scheme for TC simulations in the WRF model (orange) and for the Donelan scheme (Donelan 2018, blue), respectively.

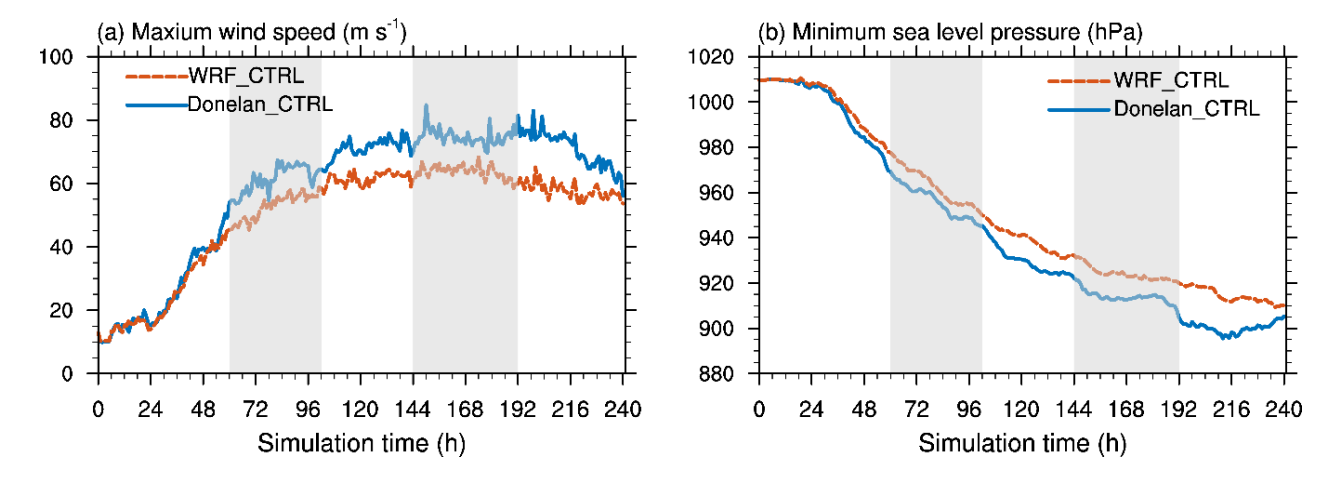


Figure 2. Time series of (a) maximum surface wind speed (m $\rm s^{-1}$) and (b) minimum sea level pressure (hPa) of the simulated TCs in experiments without the sea spray effects with the WRF $\rm C_D$ scheme (orange) and the Donelan $\rm C_D$ scheme (blue), respectively. The two stages (primary intensification and mature stages) are marked with gray shadings.

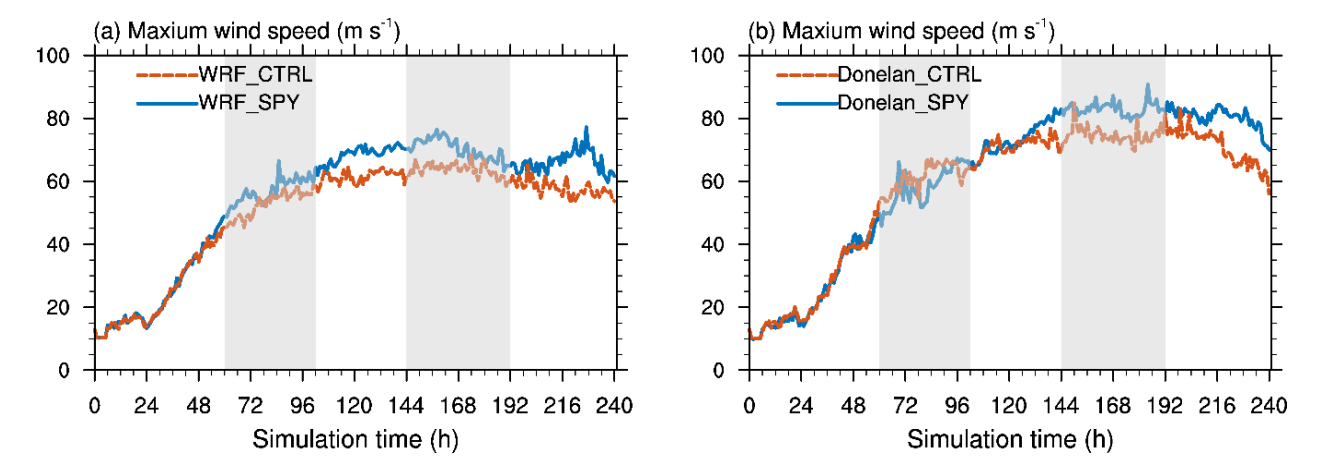


Figure 3. The time evolution of maximum 10-m wind speed (m s⁻¹) in experiments with (blue) and without (orange) the sea spray effects (a) with the WRF C_D scheme (WRF_CTRL and WRF_SPY) and (b) with the Donelan C_D scheme (Donelan_CTRL and Donelan_SPY). The two stages (primary intensification and mature stages) are marked with gray shadings.

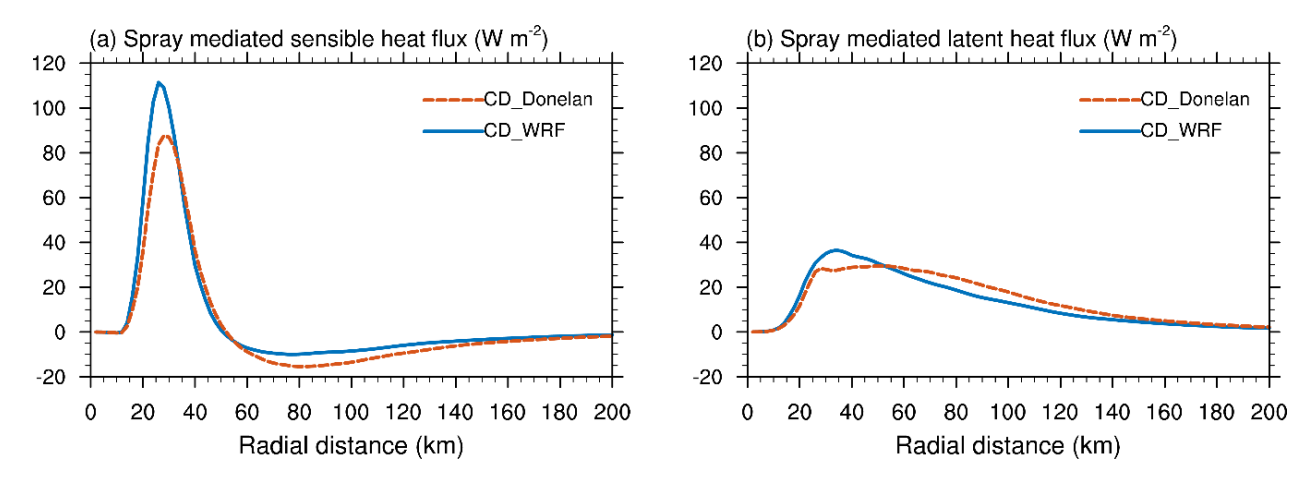


Figure 4. Spray-mediated (a) sensible heat and (b) latent heat fluxes (W m $^{-2}$) during the primary intensification stage (60–102 h) with the WRF C_D scheme (blue) and the Donelan C_D scheme (orange), respectively.

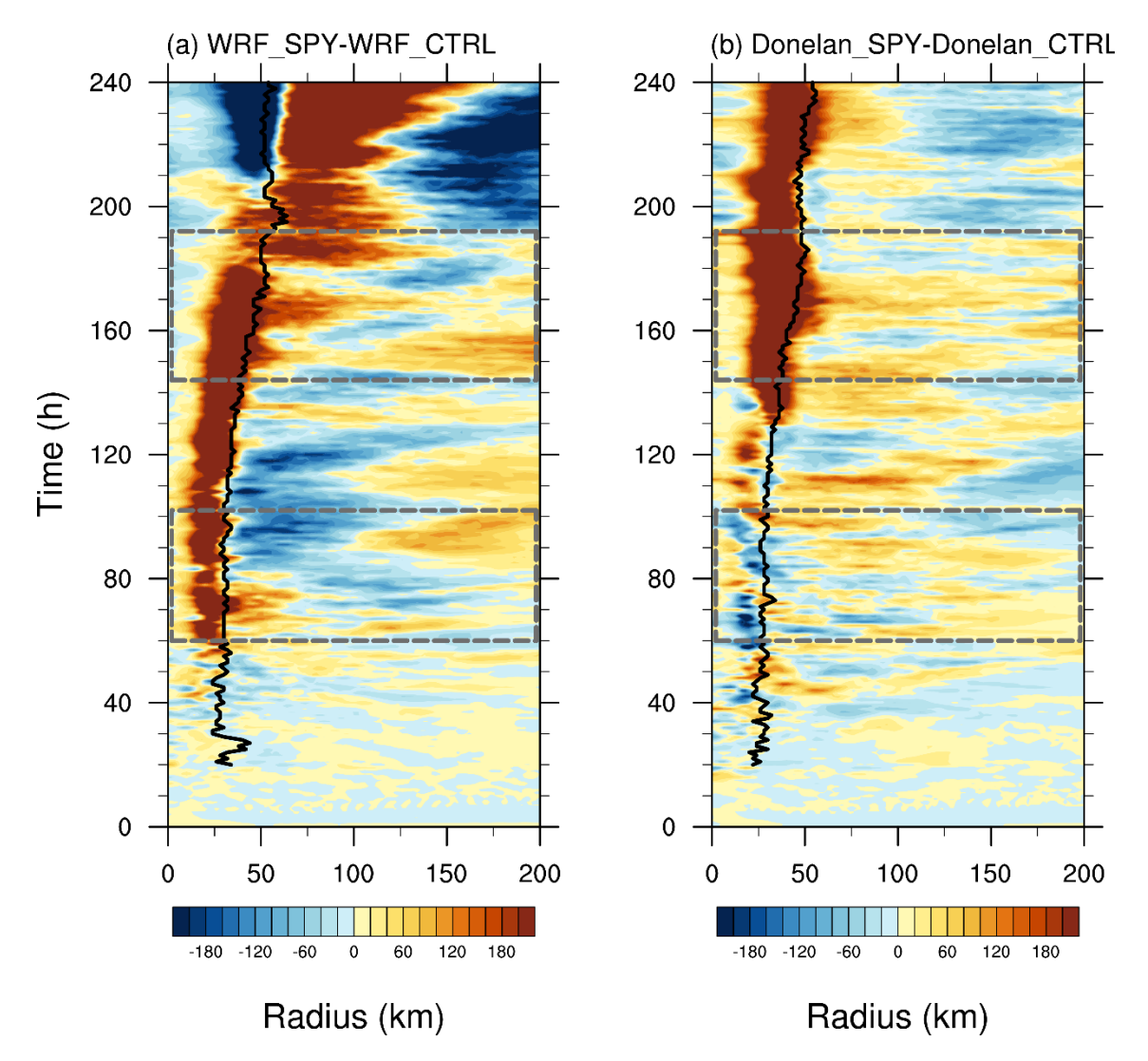


Figure 5. Radius-time cross-section of the difference in the azimuthal-mean latent heat flux (W m $^{-2}$, shading) between experiments with and without the spray effects using (a) the WRF C_D scheme and (b) the Donelan C_D scheme. Solid curves mark the RMW in the reference control experiments without the spray effects. The two stages (primary intensification and mature stages) are marked with gray lines.

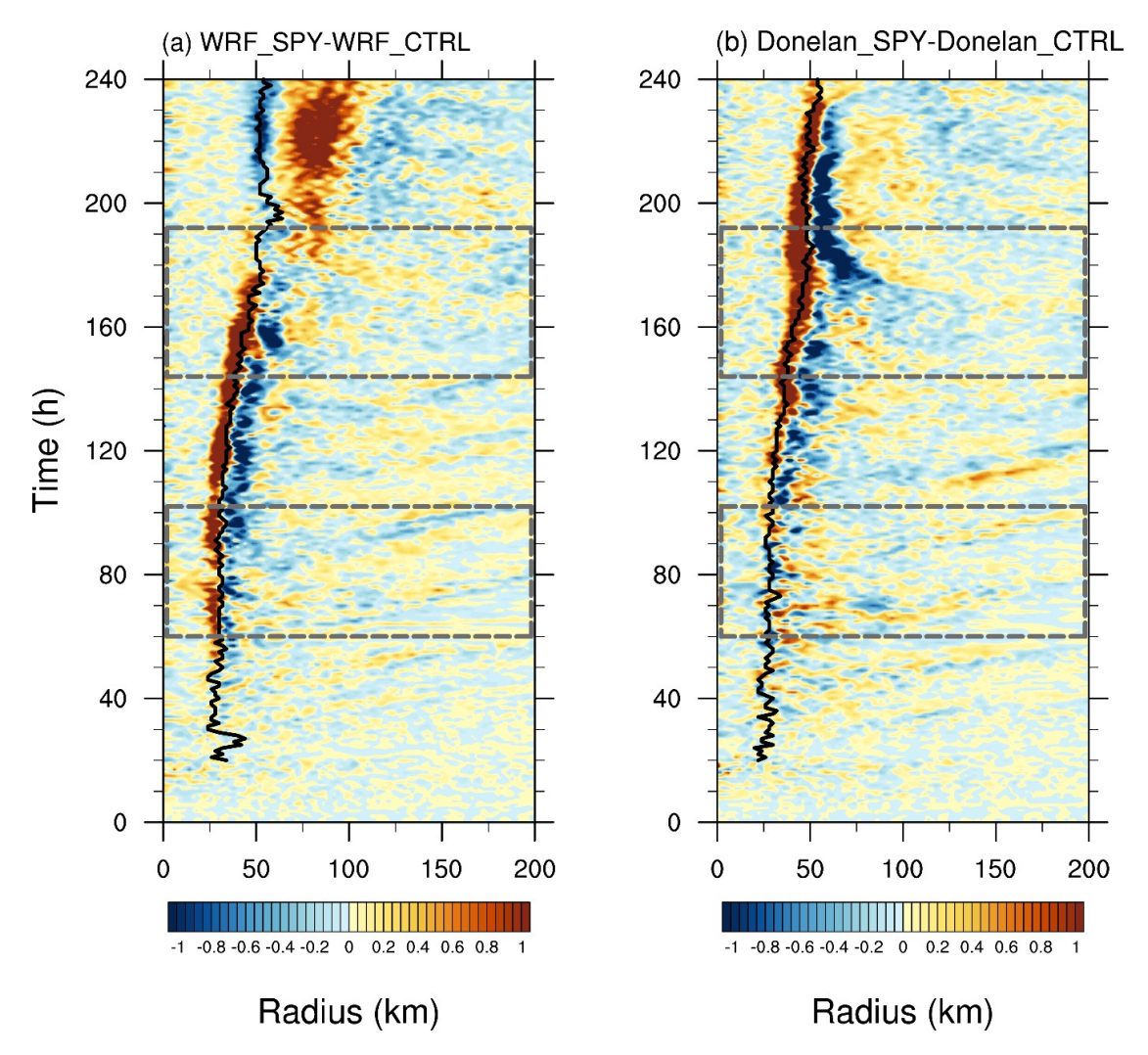


Figure 6. Radius-time cross-sections of the differences in the azimuthal-mean vertical velocity at the height of 2.3 km between experiments with and without the spray effects (m s⁻¹, shading) using (a) the WRF C_D scheme and (b) the Donelan C_D scheme. Solid curves mark the RMW in the reference control experiments without the spray effects. The two stages (primary intensification and mature stages) are marked with gray lines.

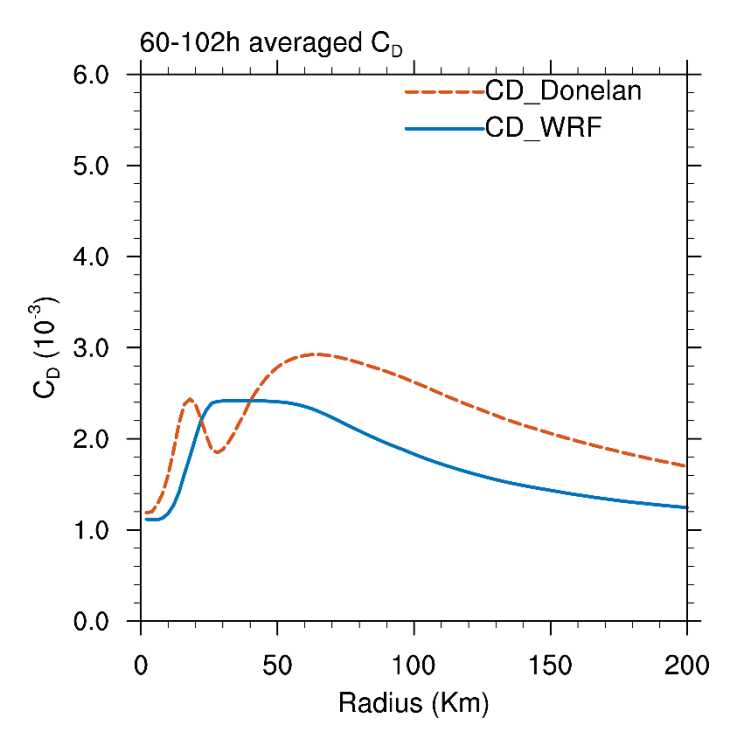


Figure 7. The radial distribution of averaged C_D during primary intensification stage (60–102 h) with WRF C_D scheme (blue) and Donelan C_D scheme (orange).

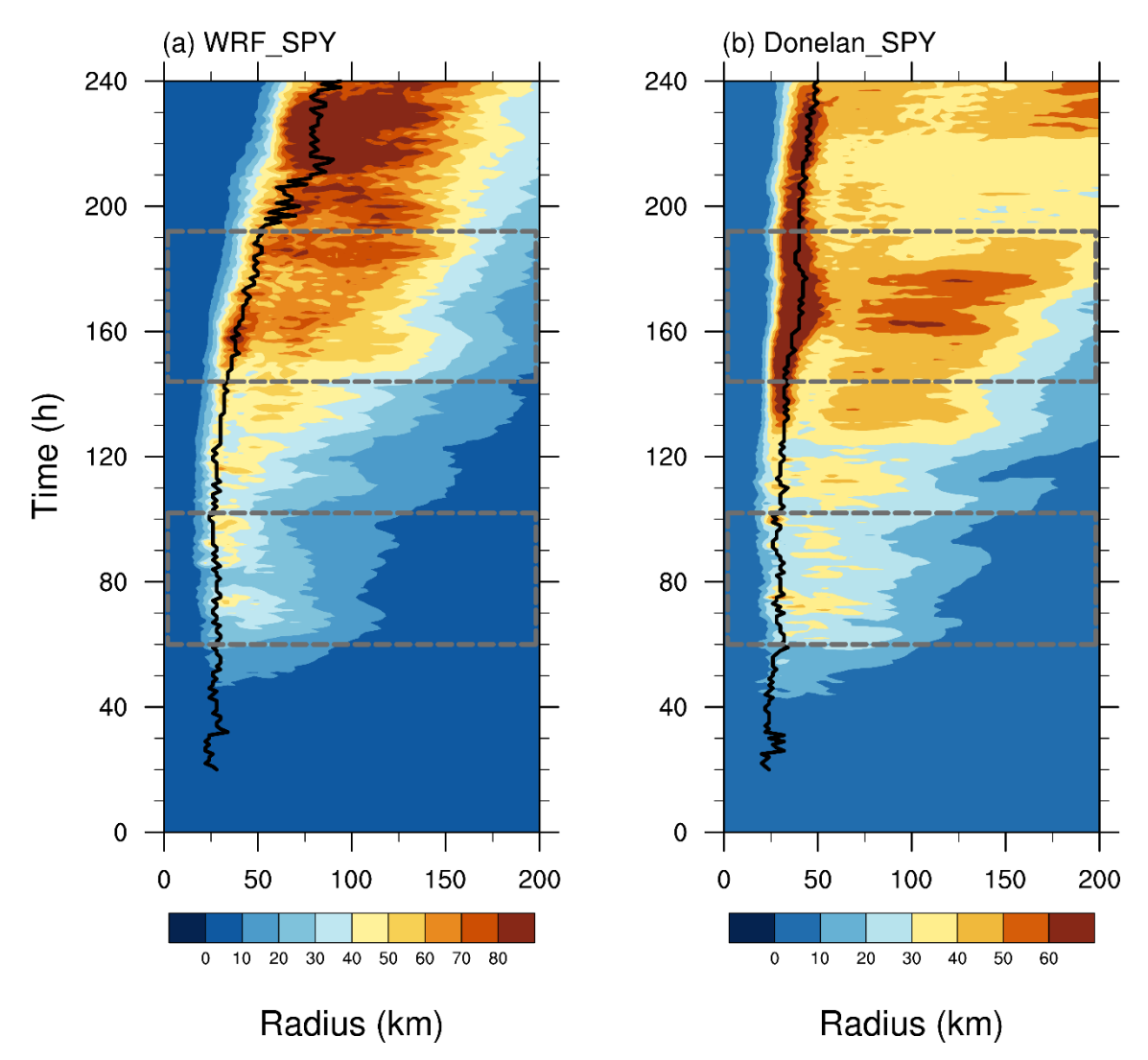


Figure 8. Radius-time cross-sections of the spray-mediated latent heat flux (W m⁻², shading) in the experiments with spray effects using (a) the WRF C_D scheme and (b) the Donelan C_D scheme. Solid curves mark the RMW in experiments. The two stages (primary intensification and mature stages) are marked with gray lines.

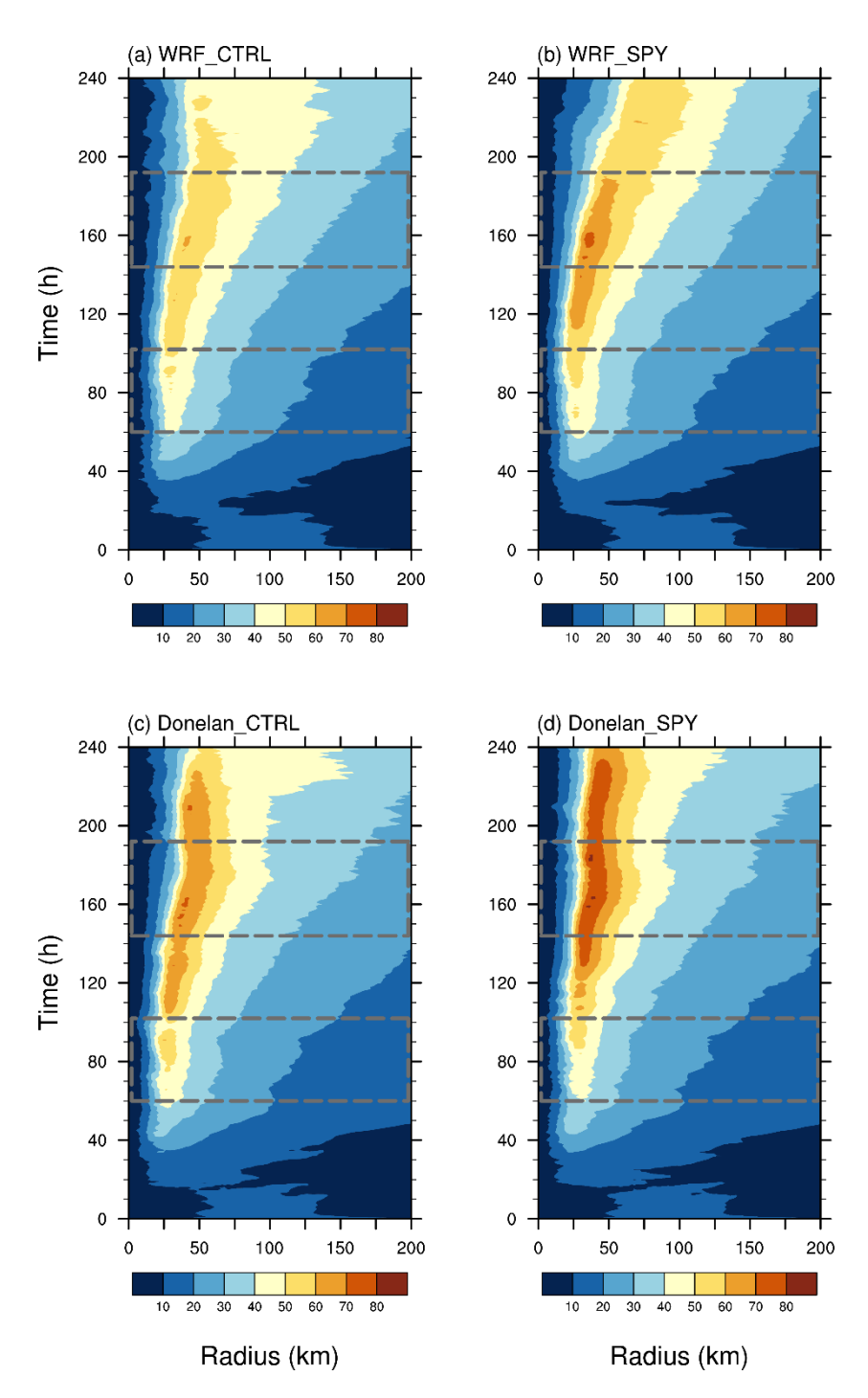


Figure 9. Hovmöller diagram of the azimuthal-mean tangential wind speed (m s⁻¹) at the lowest model level from experiments: (a) WRF_CTRL, (b) WRF_SPY, (c) Donelan_CTRL, and (d) Donelan_SPY. The two stages (primary intensification and mature stages) are marked with gray lines.

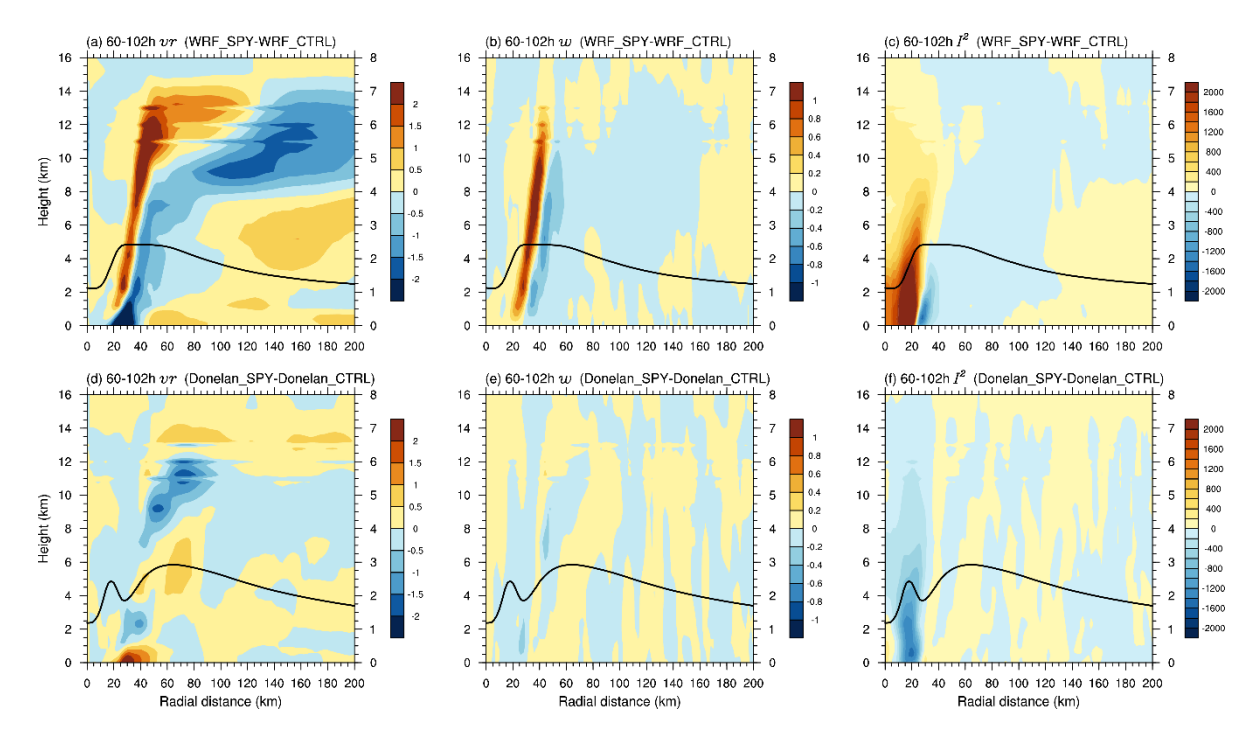


Figure 10. The differences in the azimuthal-mean radial inflow (m, s⁻¹, a and d), vertical motion (m s⁻¹, b and e) and inertial stability (s⁻¹, c and f) averaged during 60–102 h simulation period between the experiment with and without the sea spray effects with the use of the WRF C_D scheme (a-c) and of the Donelan C_D scheme (d-f). Solid curves indicate the radial distribution of C_D (10⁻³) in the corresponding control experiments. Right Y axis shows the values of C_D .

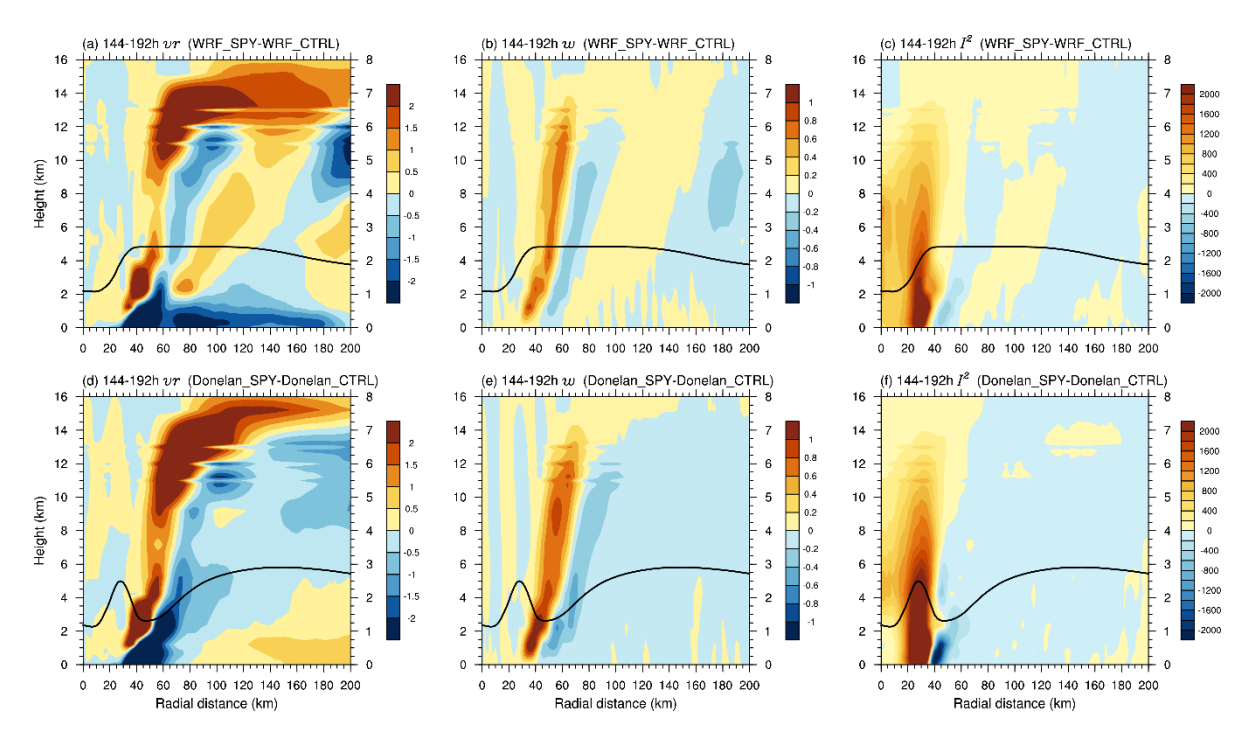


Figure 11. The same as in Fig. 10, but averaged between 144–192 h during the mature stage of the simulations.